



A model of ultrafine microstructure evolution in materials deformed by high-pressure torsion

Jan Kratochvíl^a, Martin Kružík^{b,a}, Radan Sedláček^{c,*}

^a Czech Technical University, Faculty of Civil Engineering, Department of Physics, Thákurova 7, 166 29 Prague, Czech Republic

^b Academy of Sciences of Czech Republic, Institute of Information Theory and Automation, Pod vodárenskou věží 4, 182 08 Prague, Czech Republic

^c Technische Universität München, Fakultät für Maschinenwesen Lehrstuhl für Werkstoffkunde und Werkstoffmechanik, Boltzmannstr. 15, 85747 Garching, Germany

Received 23 April 2008; received in revised form 21 August 2008; accepted 11 October 2008

Abstract

The proposed crystal plasticity model outlines a possible mechanism of a material response under severe plastic deformation as observed in high-pressure torsion experiments. A simplified version of the model based on an assumption of uniform deformation of plane-strain double slip reveals rotations of slip systems caused by the imposed shear strain. An axial compression and a shear stress of twist govern this process. The accompanied continuous reconstruction of the deformation substructure is probably one of the main reasons for the observed strengthening. Local variations in the crystal lattice orientation are responsible for the microstructure fragmentation.

© 2008 Acta Materialia Inc. Published by Elsevier Ltd. All rights reserved.

Keywords: High pressure torsion; Nanocrystalline materials; Ultrafine grained microstructure; Dislocation boundaries; Micromechanical modeling

1. Introduction

It has been well documented that severe plastic deformation produces ultrafine grained materials with extraordinary mechanical properties [1]. Very high strength and relatively good ductility are attributed to their fine microstructure. The simplest method to achieve severe plastic deformation is high-pressure torsion (HPT). This method allows the application of very high strains without interruption. The strain can be defined approximately as simple shear, $\gamma = r\theta/h$, where θ is the twist angle, h is the height of the cylindrical specimen and r is the distance from the torsion axis. Due to the dependence of γ on r , one can look at the material after a specific amount of strain in one specimen. Due to the relatively small size and structural inhomogeneity of the specimens, HPT is not very convenient as a practical technological tool. However, because of the

relative simplicity of its loading conditions, the HPT method is suitable for experimental and theoretical studies of the microstructure evolution during severe plastic deformation.

Systematic parameter studies of the microstructure evolution with increasing strain in copper, nickel and Armco iron deformed by conventional and cyclic HPT have been reported in [2,3]. The experiments were directed towards exploring the basic questions: how do the original grains fragment into much smaller structural elements? Does saturation exist in the structural refinement? How do temperature, pressure and cycling affect these phenomena? The answers to these questions provide a base for the theoretical analysis and modeling of the fragmentation process.

In the present paper, the evolution of the HPT microstructure is considered in a volume element shown in Fig. 1. In [2,3] the microstructure was observed in sections perpendicular to the radial direction (z -axis) and to the axial direction (y -axis). The observations provide detailed data on the shapes and preferred alignment of the struc-

* Corresponding author.

E-mail address: sedlacek@wkm.mw.tum.de (R. Sedláček).

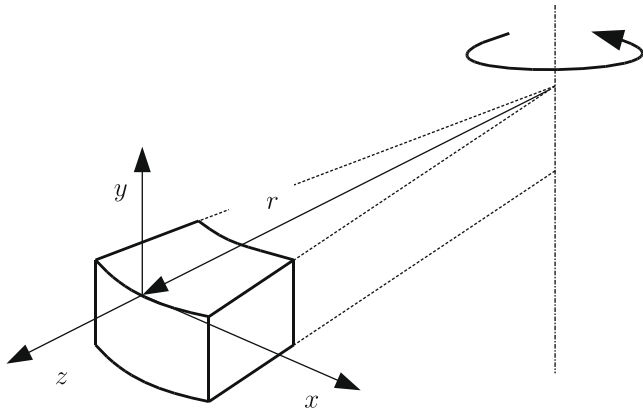


Fig. 1. A volume element exposed to HPT.

tural elements, their misorientation, size and texture. They can be summarized as follows.

1.1. Preferred alignment of structural elements

As reported in [2], for modest strain (for HPT Cu $\gamma \sim 2$) one sees rather hazily the beginning of the formation of a substructure on the micrometer scale. With increasing strain, the contrasts become more obvious and the scale of substructure decreases. For a sufficiently high strain (for HPT Cu $\gamma \sim 55$) there is no further change. A striking feature observed in the radial direction is a preferred alignment of structural elements inclined with respect to the torsion axis. For moderate strains, the apex ratio is significantly larger than 1. For larger strains, the observations indicate that the preferred alignment is not a remnant of the original grain structure. It seems that the new, smaller equiaxed structural elements are continuously formed during the deformation process. This conclusion is supported by the results of cyclic HPT of nickel and Armco iron, where it is observed that the direction of the preferred alignment changes with the reverse of the twist [3].

1.2. Misorientations

The misorientation between neighboring structural elements increases with strain and finally reaches a nearly random distribution. As reported in [2] for copper in the axial direction, there are slight misorientations for $\gamma = 2.1$, whereas large misorientations on the micrometer scale are observed at $\gamma = 4.7$. At $\gamma = 25$, large misorientations appear on the submicrometer scale. This does not change appreciably for $\gamma = 75$ and $\gamma = 250$. The misorientation between points which are farther apart than the element size becomes nearly random at even moderate strains. The boundaries between adjacent structural elements are not ‘true’ grain boundaries; frequently the term ‘non-equilibrium boundaries’ is used. Even at large misorientation angles, the elements seem to be separated by layers of finite thickness, which might be better described as arrangements of dislocations. With increasing temperature, the steady-

state boundaries between adjacent elements seem to be better defined. It is only after deformation at elevated temperatures that grain boundaries in the classic sense are observed.

1.3. Size of structural elements

As a general feature, the size of the structural elements decreases with increasing strain and reaches a steady state. Measurements on copper [2] have shown that in the axial direction, the mean size of the structural elements first decreases with increasing strain and then reaches a saturation value at a strain $\gamma > 10$. In the radial direction, one sees the formation of substructure on a scale well below $1 \mu\text{m}$, which does not seem to change beyond $\gamma = 27$. With increasing temperature, the steady-state size markedly increases and the steady-state structure is achieved at a strain as low as $\gamma < 6.8$. An increase in axial pressure leads to a somewhat finer structural size. In cyclic HPT, the strain amplitude determines the resulting structure size. For nickel and Armco iron, experiments [3] have demonstrated that after a total equivalent strain larger than approximately 20, no further refinement of the structure occurs. The greater the strain amplitude, the smaller the structural size in the saturation regime. The smallest structure size was measured for monotonically deformed samples.

1.4. Saturation

Above a certain strain, no further work hardening is observed, and in many cases there even occurs work softening. In cycling, the saturation is reached earlier in terms of number of cycles for large plastic strain amplitudes; the accumulated strain to reach saturation decreases with decreasing amplitude. The highest total strain to reach saturation is needed for monotonic deformation in HPT. In contrast to the saturations in size and mechanical strength, it seems that the increase in misorientation between neighboring elements does not saturate as quickly as the strength. Hence, one can assume that the mechanical strength is mainly determined by the size of the structural elements and not by the misorientation between them. A characteristic feature observed in the saturated state is a pronounced shear texture. One study [4] revealed that HPT nickel single crystals with different crystallographic orientation and nickel polycrystals develop a similar microstructure and microtexture in saturation. A major difference was that the stable microtexture was achieved earlier in the polycrystalline aggregates.

1.5. Deformation mechanism

The guideline for the present study has been provided by the observations reported by Hafok and Pippan [5]. Nickel samples pre-deformed by HPT in a saturated state were sheared by an additional HPT. The observed deformation

mechanism was shearing with microshear bands, which corresponds to the imposed torsion of the sample with no change in the substructure pattern. The width of the bands was about twice that of the average size of the substructure elements. From the observations, Hafok and Pippan concluded that the deformation was achieved by an intergranular glide. Grain boundary sliding was excluded as the main deformation mechanism in the explored HPT process.

For the interpretation of the fragmentation process, we employ the framework of crystal plasticity summarized in Section 2. In Sections 3 and 4, the considerations are restricted to spatially homogeneous plane-strain, rigid-plastic deformation carried by double slip. A rate-independent material response is considered. Despite these simplifications, the idealized framework provides a possible explanation for some of the observations summarized above. The basic feature of the model is a rotation of the slip systems carrying the imposed HPT strain. The slip activity is governed by the shear stress imposed by torsion and by axial compression. In Section 5 we suggest that the results of the recent paper [6] can be employed in a qualitative analysis of the fragmentation process. In [6], formation of a structural element pattern (misoriented cell pattern) was explained as the result of a trend to reduce energetically costly multislip. In the context of HPT, this means that at each orientation of the slip systems there is a tendency to build the corresponding pattern. The rotation of the slip systems causes a continuous reconstruction of the pattern. The effect leads to an increase in the dislocation density and enhanced hardening. In the deformation process, the orientation of the slip systems asymptotically approaches a steady state related to the saturation effect.

2. Crystal plasticity

The crystal plasticity equations were introduced in such classic papers as Refs. [7,8]. Here, the rigid-plastic approximation to the kinematics of crystal plasticity elaborated in [9] is considered. The constitutive assumption adopted is a rate-independent material response.

2.1. Kinematics

Each material point can be identified by its position in a reference configuration. The point which was at position \mathbf{X} in the reference configuration is in the current configuration in time t in the position $\mathbf{x}(\mathbf{X}, t)$. The difference $\mathbf{u} = \mathbf{x} - \mathbf{X}$ is the displacement of the material point \mathbf{X} . The deformation of an infinitesimal material fiber from the reference to the current configuration,

$$d\mathbf{x} = \mathbf{F} d\mathbf{X}. \quad (1)$$

Assuming that $\mathbf{x}(\mathbf{X}, t)$ is a continuous and differentiable vector field, this transformation can be introduced as the deformation gradient $\mathbf{F} = \partial\mathbf{x}/\partial\mathbf{X} = \mathbf{I} + \partial\mathbf{u}/\partial\mathbf{X}$, where \mathbf{I} is

the second-order identity tensor. In the rigid-plastic approximation the crystal lattice can (rigidly) rotate but is not (elastically) deformed. The plastic deformation of a crystal can be notionally decomposed in two steps. First, the material flows through the crystal lattice by shearing along active slip systems to reach an intermediate configuration. This step is described by the plastic deformation gradient \mathbf{F}^p . Second, the plastic deformation \mathbf{F}^p is followed by a rigid rotation \mathbf{R} of the lattice. The corresponding decomposition reads

$$\mathbf{F} = \mathbf{R}\mathbf{F}^p. \quad (2)$$

We note in passing that in the case of inhomogeneous plastic deformation \mathbf{F}^p , the lattice rotation \mathbf{R} can re-establish the compatibility of the overall material deformation. This process leads, for example, to formation of misoriented dislocation cells (cf. [9,10,6]).

The velocity \mathbf{v} of a material point is given by the (Lagrangian) derivative of its position, $\mathbf{v}(\mathbf{x}, t) = \dot{\mathbf{x}}(\mathbf{X}, t)$. Now, we perform the time derivative of Eq. (1)

$$d\dot{\mathbf{x}} = \dot{\mathbf{F}} d\mathbf{X} = \frac{\partial\mathbf{v}(\mathbf{x}, t)}{\partial\mathbf{X}} d\mathbf{X} = \frac{\partial\mathbf{v}}{\partial\mathbf{x}} \mathbf{F} \mathbf{F}^{-1} d\mathbf{x} = \mathbf{L} d\mathbf{x},$$

where $\mathbf{L}(\mathbf{x}, t) = \dot{\mathbf{F}}\mathbf{F}^{-1} = \partial\mathbf{v}/\partial\mathbf{x}$ is the velocity gradient. Using Eq. (2), the latter can be decomposed¹ as

$$\mathbf{L} = \mathbf{L}^p + \boldsymbol{\Omega}, \quad (3)$$

where \mathbf{L}^p is the rate of plastic distortion in the current configuration and $\boldsymbol{\Omega}$ is the lattice spin. The rate of plastic distortion, which represents the plastic flow in the current configuration, can be written in terms of shear strain rates $\dot{\gamma}^{(i)}(\mathbf{x}, t)$ on the active slip systems (i), $i = 1, 2, \dots, I$,

$$\mathbf{L}^p = \sum_{i=1}^I \dot{\gamma}^{(i)} \mathbf{s}^{(i)} \otimes \mathbf{m}^{(i)}. \quad (4)$$

The i th slip system is defined in the reference configuration by the unit vector in the direction of slip $\mathbf{s}_0^{(i)}(\mathbf{X}, t)$ and the unit normal to the glide plane $\mathbf{m}_0^{(i)}(\mathbf{X}, t)$. The lattice vectors $\mathbf{s}^{(i)}$ and $\mathbf{m}^{(i)}$ rotate rigidly by virtue of the deformation gradient \mathbf{F} from the reference into current configuration

$$\mathbf{s}^{(i)} = \mathbf{R}\mathbf{s}_0^{(i)}, \quad \mathbf{m}^{(i)} = \mathbf{R}\mathbf{m}_0^{(i)}. \quad (5)$$

From the time derivation of Eq. (5), it follows that the current lattice vectors spin rigidly with the lattice²

$$\dot{\mathbf{s}}^{(i)} = \boldsymbol{\Omega}\mathbf{s}^{(i)}, \quad \dot{\mathbf{m}}^{(i)} = \boldsymbol{\Omega}\mathbf{m}^{(i)} \quad (6)$$

¹ In detail: $\mathbf{L} = \dot{\mathbf{F}}\mathbf{F}^{-1} = \mathbf{R}\dot{\mathbf{F}}^p(\mathbf{F}^p)^{-1}\mathbf{R}^T + \dot{\mathbf{R}}\mathbf{R}^T$, where $\dot{\mathbf{F}}^p(\mathbf{F}^p)^{-1}$ is the rate of plastic distortion in the reference lattice, $\mathbf{R}\dot{\mathbf{F}}^p(\mathbf{F}^p)^{-1}\mathbf{R}^T = \mathbf{L}^p$ is the rate of plastic distortion rotated with the lattice into the current configuration and $\dot{\mathbf{R}}\mathbf{R}^T = \boldsymbol{\Omega}$ is the lattice spin.

² Explicitly: $\dot{\mathbf{s}}^i = \dot{\mathbf{R}}\mathbf{s}_0^{(i)} = \dot{\mathbf{R}}\mathbf{R}^T\mathbf{s}^{(i)} = \boldsymbol{\Omega}\mathbf{s}^{(i)}$ and $\dot{\mathbf{m}}^i = \dot{\mathbf{R}}\mathbf{m}_0^{(i)} = \dot{\mathbf{R}}\mathbf{R}^T\mathbf{m}^{(i)} = \boldsymbol{\Omega}\mathbf{m}^{(i)}$.

2.2. Constitutive model

The plastic shear rates $\dot{\gamma}^{(i)}$ in the current slip systems (i) are driven by resolved shear stresses $\tau^{(i)}$:

$$\dot{\gamma}^{(i)} = \lambda^{(i)} \text{sign} \tau^{(i)}, \quad (7)$$

where $\lambda^{(i)} \geq 0$ are the plastic multipliers. Eq. (7) is the flow rule. The resolved shear stresses are related to the Cauchy stress $\mathbf{S}(\mathbf{x}, t)$ by the relation

$$\tau^{(i)} = \mathbf{s}^{(i)} \cdot \mathbf{S} \mathbf{m}^{(i)}. \quad (8)$$

A slip system (i) can be activated only if the magnitude of the resolved shear stress $\tau^{(i)}$ reaches the critical value (yield stress) $\tau_y^{(i)}$:

$$|\tau^{(i)}| = \tau_y^{(i)}. \quad (9)$$

This is the yield condition. The critical resolved shear stress, i.e. the hardness of a slip system, has a character of a friction, so that $\tau_y^{(i)} > 0$. The rate of change in $\tau_y^{(i)}$, i.e. the hardening of the i th slip system, can be written in the standard form

$$\dot{\tau}_y^{(i)} = \sum_{j=1}^I H_{ij} |\dot{\gamma}^{(j)}|. \quad (10)$$

The hardening matrix \mathbf{H} is deformation-history dependent and in general not symmetric.

3. Lattice rotations

The analysis of lattice rotations in torsion performed in Section 3.2 below is inspired by the detailed study (experimental and computational) of structure and micromechanisms of strain localization process during plane-strain compression (PSC) of face-centered cubic single crystals and polycrystals in a channel die performed by Harren et al. [8]. We recall the basic results of the latter analysis first.

3.1. Symmetric double slip in plane-strain compression

X-ray measurements were carried out by Harren et al. [8] to determine the lattice reorientation of the single crystals of various initial crystallographic orientations before macroscopic shear bands appeared, i.e. up to the engineering compression strain $\approx 0.3 - 0.9$. It was observed that, except for crystals oriented symmetrically with respect to the compression and extension axes, the crystals exhibited an overall common behavior. After yield, all these crystals started to reorient in such a way that their crystallographic direction $[110]$ approached the compression axis and the direction $[001]$ became parallel to the extension axis along the channel, i.e. these reorientations tend to bring the crystals toward the $(110)[001]$ orientation. The $(110)[001]$ geometry coincides with a stable state of symmetric slip on four slip systems: $(111)[10\bar{1}]$, $(111)[01\bar{1}]$ and $(11\bar{1})[101]$, $(11\bar{1})[011]$. The net shearing systems associated with this symmetric state are then $[11\bar{2}]$ in (111) and $[112]$

in $(11\bar{1})$, and hence the resulting deformation of this symmetric state is aligned with the channel. So, for these crystals, as the deformation proceeds, this state of plane-strain crystallographic deformation is approached.

In order to simulate the compression tests of single crystals, Harren et al. [8] employed a two-dimensional single crystal model with the two considered slip systems $(111)[11\bar{2}]$ and $(11\bar{1})[112]$. Its reference configuration is shown in Fig. 2. The orientation of the slip systems with respect to compression axis is $\phi = \arccos\{([110]/\sqrt{2}) \cdot ([112]/\sqrt{6})\} \approx 55^\circ$, Fig. 2. The experimental observations and the computed deformation response were in close agreement.

In the PSC tests of polycrystals [8], the observed micromechanics demonstrated that highly nonuniform grain deformations and lattice rotations provided a ‘crystallographic path’ that allowed slip to be transmitted across grain boundaries. The FEM calculations based on a plane-strain model of the polycrystal have been consistent with the experimental observations. The study revealed that in the early stages of deformation the grains tend to rotate toward an ideal texture orientation. This increases the global anisotropy of the polycrystal, but decreases the local heterogeneity, since the grain lattices all tend to become more or less aligned with each other. As the deformation continues, the alignment tends to decrease the grain boundary lattice misorientations, thus allowing for an easier transmission of slip. As the rotations toward the ideal texture proceed, the inherently nonuniform deformations within the grains precipitate the formation of grain level shearing modes. The shearing within a single grain often behaves in a similar manner to that within the single crystals.

Inspired by this successful model, we use a simple crystallographic double-slip plane-strain approximation for the

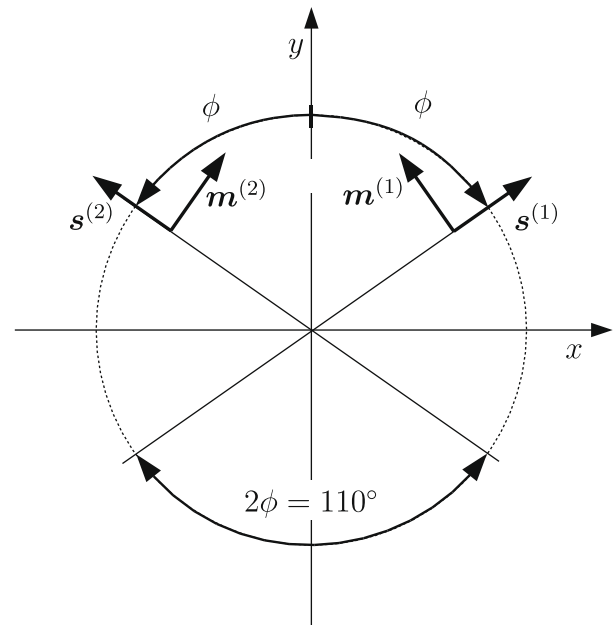


Fig. 2. Schematics of plane-strain symmetric double slip with $\phi = 55^\circ$.

analysis of the slip systems behavior in torsion. However, we apply the simple model to the PSC first, to see if it predicts the rotation of the slip systems towards the symmetric double slip mode assumed by Harren et al. [8].

We consider an (in general) asymmetric double slip in a homogeneous single crystal and analyze the lattice rotations. The unit vectors in the directions of slip $\mathbf{s}^{(i)}$ and the unit normals to the slip planes $\mathbf{m}^{(i)}$, $i = 1, 2$, in the current configuration are

$$\begin{aligned} \mathbf{s}^{(1)} &= (\sin \phi_1, \cos \phi_1), & \mathbf{m}^{(1)} &= (-\cos \phi_1, \sin \phi_1), \\ \mathbf{s}^{(2)} &= (-\sin \phi_2, \cos \phi_2), & \mathbf{m}^{(2)} &= (\cos \phi_2, \sin \phi_2), \end{aligned} \quad (11)$$

where ϕ_1, ϕ_2 are the angles of the slip directions $\mathbf{s}^{(1)}, \mathbf{s}^{(2)}$ with respect to y -axis, as indicated in Fig. 3, and $\phi_1 + \phi_2 = 2\phi$, where ϕ is a characteristic of the slip crystallography. In the present case we take $\phi = 35^\circ$ (the complementary choice $\phi = 55^\circ$ leads to equivalent results). It is important to note that from Eqs. (6) and (11) we get the rate of change in the slip directions

$$\dot{\phi}_1 = -\dot{\phi}_2 = \Omega_{xy}. \quad (12)$$

According to Eq. (3) the velocity gradient \mathbf{L} consists of the rate of plastic distortion \mathbf{L}^P due to the shear strain rates on the considered two slip systems, and the corresponding lattice spin $\mathbf{\Omega}$. Using Eq. (4), the velocity gradient for (in general asymmetric) double slip in the form $\mathbf{L} = \mathbf{L}^P + \mathbf{\Omega}$ results in

$$\begin{aligned} \begin{pmatrix} L_{xx} & L_{xy} \\ L_{yx} & L_{yy} \end{pmatrix} &= \frac{\dot{\gamma}^{(1)}}{2} \begin{pmatrix} -\sin 2\phi_1 & 2\sin^2 \phi_1 \\ -2\cos^2 \phi_1 & \sin 2\phi_1 \end{pmatrix} \\ &+ \frac{\dot{\gamma}^{(2)}}{2} \begin{pmatrix} -\sin 2\phi_2 & -2\sin^2 \phi_2 \\ 2\cos^2 \phi_2 & \sin 2\phi_2 \end{pmatrix} + \begin{pmatrix} 0 & \Omega_{xy} \\ -\Omega_{xy} & 0 \end{pmatrix}. \end{aligned} \quad (13)$$

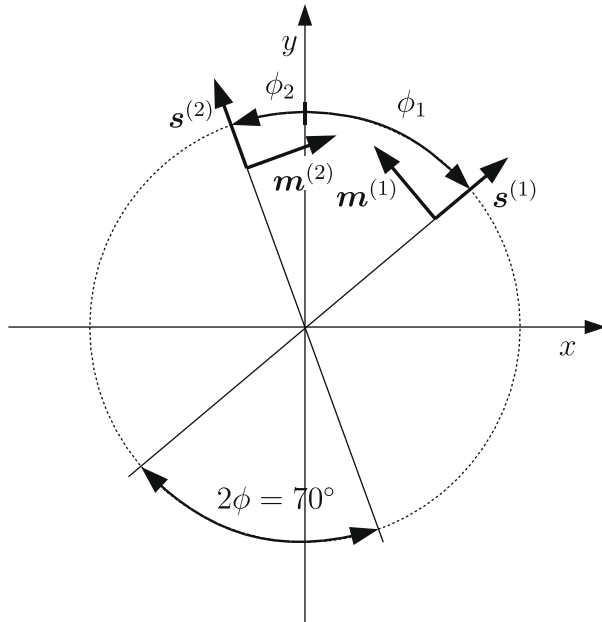


Fig. 3. Schematics of asymmetric double slip with $2\phi = 70^\circ$.

In the case of PSC, the deformation mode is characterized by a compression in the y direction, accompanied, because of the incompressibility, by extension in the x direction. The corresponding deformation gradient \mathbf{F} reads

$$\begin{pmatrix} x \\ y \end{pmatrix} = \begin{pmatrix} F_{xx} & 0 \\ 0 & 1/F_{xx} \end{pmatrix} \begin{pmatrix} X \\ Y \end{pmatrix},$$

and the velocity gradient $\mathbf{L} = \dot{\mathbf{F}}\mathbf{F}^{-1}$ results as

$$\mathbf{L} = \begin{pmatrix} L_{xx} & 0 \\ 0 & -L_{xx} \end{pmatrix}, \quad (14)$$

where $L_{xx} = \dot{F}_{xx}/F_{xx}$. From Eqs. (13) and 14, we get the following equations for Ω_{xy} and $\dot{\gamma}^{(i)}$, $i = 1, 2$:

$$\begin{aligned} \Omega_{xy} &= \frac{\sin(\phi_1 - \phi_2)}{\cos 2\phi} L_{xx}, & \dot{\gamma}^{(1)} &= \frac{-2\cos 2\phi_2}{\sin 4\phi} L_{xx}, & \dot{\gamma}^{(2)} \\ &= \frac{-2\cos 2\phi_1}{\sin 4\phi} L_{xx}. \end{aligned} \quad (15)$$

These variables are plotted as functions of $\phi_1 \in [-90^\circ, 90^\circ]$ in Fig. 4. An asymmetric double slip, Fig. 3, develops towards the orientation with $\phi_1 = -55^\circ$, i.e. $\phi_2 = 125^\circ$. This orientation corresponds to the symmetric double slip assumed by Harren et al. [8] which is sketched in Fig. 2. It is stable, which means that $\Omega_{xy} = 0$ for $\phi_1 = -55^\circ$ and the rate of rotation Ω_{xy} for disturbed orientations is such that it brings the crystal back to this orientation (cf. Fig. 4). Note that the complementary symmetric double slip orientation, $\phi_1 = 35^\circ$, $\phi_2 = 35^\circ$, $\Omega_{xy} = 0$, is unstable, since a disturbance of this orientation grows. There is one more stable and one more unstable orientation outside

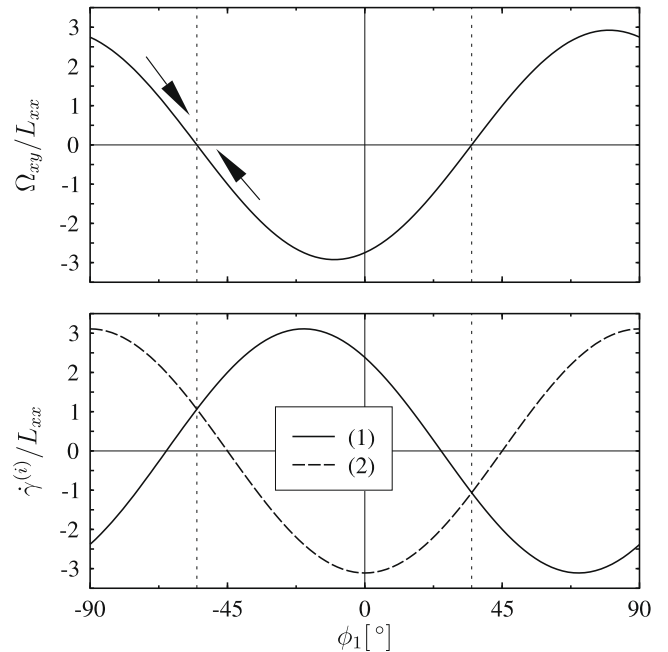


Fig. 4. Plot of Eq. (15), representing double slip in PSC for $2\phi = 70^\circ$. The vertical dotted lines mark the orientations with $\Omega_{xy} = 0$, while the arrows indicate the development towards the stable orientation. (1) and (2) indicate the slip systems.

the scope of the graph in Fig. 4 which are equivalent to the two discussed. The present analysis thus certifies the result of Harren et al. [8]. In the following section, we apply the same analysis to shearing of a volume element which occurs in the HPT.

3.2. Asymptotic single slip in torsion

Consider a rectangular volume element which idealizes the geometry of the cylindrical volume element shown in Fig. 1. The front face of the rectangular element is perpendicular to the radial direction, which is taken as the z -axis of a local coordinate system $\mathbf{x} = (x, y, z)$. The other faces are perpendicular to the x and y axes. The x coordinate is perpendicular to the plane of the radial and axial directions, and the y coordinate is parallel to the torsion axis. The volume element is assumed to be in plane-strain conditions in the plane perpendicular to the radial direction. In this idealization, a variation of the stress and strain fields, and the fragmentation in the radial direction are excluded from the consideration. The excluded features are commented later in Section 5.

We assume that the considered volume element is a part of single crystal deformed in double slip. In this section, a uniform deformation is analyzed, i.e. the field variables of crystal plasticity introduced in Section 2 are spatially homogeneous and depend on time t only. In the uniform plane-strain simplification of the HPT, the volume element is subjected to simple shear

$$\begin{pmatrix} x \\ y \end{pmatrix} = \begin{pmatrix} 1 & F_{xy} \\ 0 & 1 \end{pmatrix} \begin{pmatrix} X \\ Y \end{pmatrix}.$$

The corresponding velocity gradient $\mathbf{L} = \dot{\mathbf{F}}\mathbf{F}^{-1}$ is

$$\mathbf{L} = \begin{pmatrix} 0 & L_{xy} \\ 0 & 0 \end{pmatrix}, \quad (16)$$

where $L_{xy} = \dot{F}_{xy}$ is determined by the imposed torsion. The shear flow rate L_{xy} can be defined approximately as $L_{xy} \approx r\dot{\theta}/h$, where θ is the twist angle, h is the height of the cylindrical specimen and r is the distance from the torsion axis (cf. Section 1).

Eq. (13) with \mathbf{L} in the form (16) yields the following equations for Ω_{xy} and $\dot{\gamma}^{(i)}$, $i = 1, 2$:

$$\begin{aligned} \Omega_{xy} &= \frac{\cos \phi_1 \cos \phi_2}{\cos 2\phi} L_{xy}, & \dot{\gamma}^{(1)} &= -\frac{\sin 2\phi_2}{\sin 4\phi} L_{xy}, \\ \dot{\gamma}^{(2)} &= \frac{\sin 2\phi_1}{\sin 4\phi} L_{xy}. \end{aligned} \quad (17)$$

Plots of Eq. (17) are shown in Fig. 5 for $\phi_1 \in [-90^\circ, 90^\circ]$, that is $\phi_2 \in [160^\circ, -20^\circ]$. From these graphs, it is seen that the double slip develops towards the single slip, i.e. either $\dot{\gamma}^{(1)}$ or $\dot{\gamma}^{(2)}$ vanishes, for various orientations. Interesting, however, are the single slip regimes where additionally $\Omega_{xy} = \dot{\phi}_1 = 0$, because these, once reached, could persist. This occurs for $\phi_1 = -90, -20, 90$ and 160° , the latter being outside the scope of the diagram. From these four

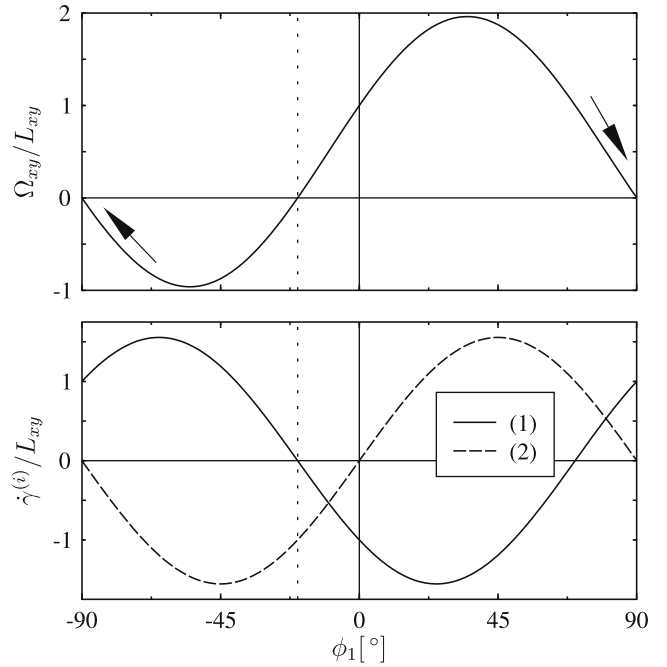


Fig. 5. Plot of Eq. (17) representing double slip in simple shear with $2\phi = 70^\circ$. The evolution towards the stable single-slip orientations is indicated by arrows. (1) and (2) indicate the slip systems.

regimes, only two, $\phi_1 = -90$ and 90° , are stable. This means that if there is a disturbance of the single slip regime, the lattice spin acts against the disturbance, thus returning the crystal orientation to the single slip one. The other two are unstable: there, a disturbance grows even further by virtue of the lattice spin. Thus the value $\phi_1 = -20^\circ$ represents a borderline: for $\phi_1 < -20^\circ$ the slip systems rotate towards the stable state $\phi_1 = -90^\circ$, for $\phi_1 > -20^\circ$ they rotate towards $\phi_1 = 90^\circ$. Similar for $\phi_1 = 160^\circ$.

However, to reach the stable single slip, an infinite deformation, $F_{xy} \rightarrow \infty$, is necessary. The reason for this is that, in the considered case of simple shear of the volume element, we get from $\dot{\mathbf{F}} = \mathbf{L}\mathbf{F}$ that $\dot{F}_{xy} = L_{xy}$ and from (6), (11) and (17)

$$\dot{\phi}_1 = -\dot{\phi}_2 = \Omega_{xy} = \dot{F}_{xy} \frac{\cos \phi_1 \cos \phi_2}{\cos 2\phi}. \quad (18)$$

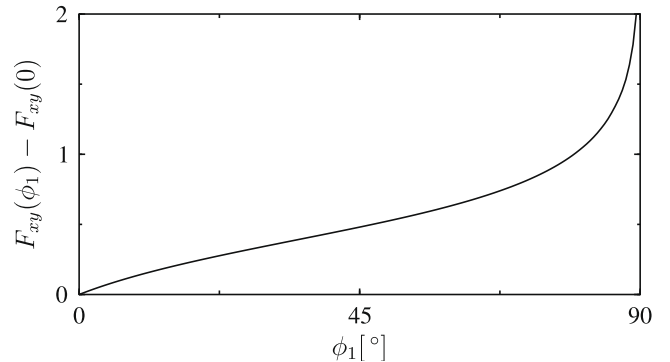


Fig. 6. Plot obtained by integration of Eq. (18) with $2\phi = 70^\circ$.

The singularity of F_{xy} at $\phi_1 = 90^\circ$ is shown in the graph in Fig. 6, which was obtained by integration of Eq. (18). Thus, the single slip orientation in a volume element deformed in plane-strain simple shear in double slip is reached asymptotically.

4. Stress

In HPT experiments, an axial torque is combined with a high axial compression. Under these loading conditions, the sample is exposed to a shear stress, to an axial compression and to a hydrostatic pressure. The shear stress is induced by the applied torque. The stress in the sample imposed by the applied axial compression of the HPT tool can be divided into the axial compression stress and the hydrostatic pressure. The reason for the partition is that, up to the current flow stress, the tested material of the specimen together with the HPT tool behave as a body consisting of two elastic parts in contact exposed to a compression. Only the part of the stress in the sample stemming from the applied compression which exceeds the current flow stress acquires a hydrostatic character, because the material of the sample flows. FEM simulations of the HPT experiments [11] confirmed such a stress field interpretation.

In the assumed plane-strain conditions, the volume element is exposed to a uniform Cauchy stress $\mathbf{S}(t)$:

$$\mathbf{S} = \begin{pmatrix} -p & S_{xy} & 0 \\ S_{xy} & -p + S_{yy}^c & 0 \\ 0 & 0 & -p \end{pmatrix}, \quad (19)$$

where S_{xy} is the shear stress, S_{yy}^c is the axial compression and p is the hydrostatic pressure. In Eq. (19), we require that the pressure be high enough so that $-p + S_{yy}^c < 0$, to preserve a non-sliding contact between the specimen and the tool.

Slip in the i th slip system is driven by the resolved shear stress $\tau^{(i)}$ given by Eq. (8). From Eqs. 5, 11 and 19, we get the stresses as

$$\begin{aligned} \tau^{(1)} &= -S_{xy} \cos 2\phi_1 + \frac{S_{yy}^c}{2} \sin 2\phi_1, & \tau^{(2)} \\ &= S_{xy} \cos 2\phi_2 + \frac{S_{yy}^c}{2} \sin 2\phi_2, \end{aligned} \quad (20)$$

which implies

$$\begin{aligned} S_{xy} &= \frac{\tau^{(2)} \sin 2\phi_1 - \tau^{(1)} \sin 2\phi_2}{\sin 4\phi}, & S_{yy}^c \\ &= 2 \frac{\tau^{(2)} \cos 2\phi_1 + \tau^{(1)} \cos 2\phi_2}{\sin 4\phi}. \end{aligned} \quad (21)$$

The stress components S_{xy} and S_{yy}^c are necessary to create simultaneously the resolved shear stresses $\tau^{(1)}$ and $\tau^{(2)}$ in the two slip systems. We want to determine the dependence of the stress components S_{xy} and S_{yy}^c on the crystal orientation (represented by ϕ_1) such that the double slip persists; that is, both slip systems remain active. In view of Fig. 5, this

is the case for all orientations except those where $\text{sign} \dot{\gamma}^{(i)}$ changes. In these singular points, one of the slip systems temporarily switches off and the resolved shear stress at this system jumps across the elastic range in the other direction. The necessary jump in the resolved shear stress may require a non-smoothness or even a jump in the dependence of the stress components S_{xy} and S_{yy}^c on the crystal orientation. From the flow rule (7) and yield condition (9), it can be deduced that a slip system remains active if and only if

$$\tau^{(i)} = \tau_y^{(i)} \text{sign} \dot{\gamma}^{(i)}. \quad (22)$$

The dependence of $\text{sign} \dot{\gamma}^{(i)}$ on ϕ_1 follows from Fig. 5. Assuming for simplicity that $\tau_y^{(1)} = \tau_y^{(2)} = \tau_y$ and substituting Eq. (22) in (21), we get the graphs of the components of the stress response S_{xy}/τ_y and $S_{yy}^c/2\tau_y$ shown in Fig. 7. As seen in the figure, in the orientations where $\text{sign} \dot{\gamma}^{(i)}$ changes while the crystal rotates, the resolved shear stress needs to jump over the elastic range to activate the i th slip system in the other direction. Note, however, that in the present case (and in the range of the diagram in Fig. 7) these critical orientations are $\phi_1 = 0$ and $\phi_1 = 70^\circ$ (i.e. $\phi_2 = 0$) only. The orientations $\phi_1 = \pm 90^\circ$ represent the stable limit states approached asymptotically that cannot be crossed, and $\phi_1 = -20^\circ$ (i.e. $\phi_2 = 90^\circ$) is the borderline that cannot be crossed either, because the rotation Ω_{xy} always directs from this orientation away. From Eqs. (17)_{2,3}, (21) and (22), it follows that in the points of change in $\text{sign} \dot{\gamma}^{(i)}$ the shear stress component S_{xy} exhibits sharp bends, whereas the jumps in S_{yy}^c are

$$\Delta S_{yy}^c(0) = \frac{4\tau_y^{(2)}}{\sin 4\phi}, \quad \Delta S_{yy}^c(70^\circ) = \frac{4\tau_y^{(1)}}{\sin 4\phi}. \quad (23)$$

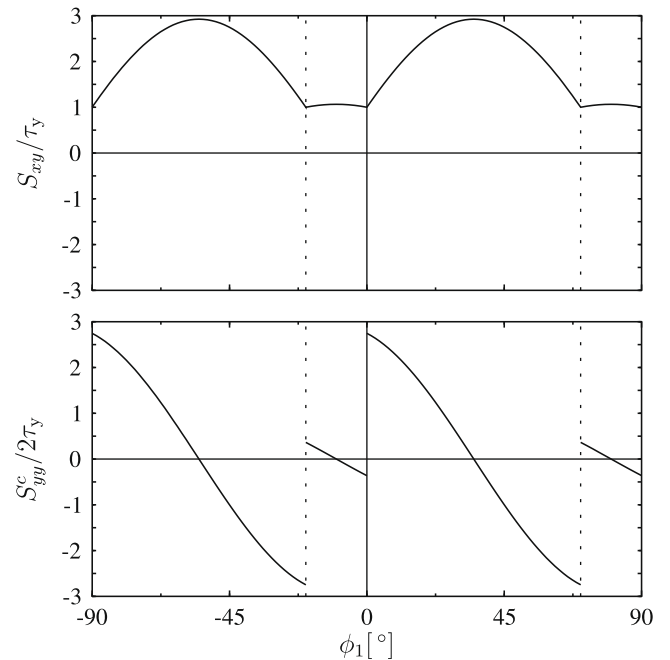


Fig. 7. Plot of Eq. (21) with the signs of $\tau^{(i)}$ determined by Eq. (22). The vertical dotted lines denote the change of sign in $\dot{\gamma}^{(i)}$.

It is interesting to note that, depending on the crystal orientation, the stress components S_{yy}^c in the HPT sample that is exposed to a strong axial compression can be either positive or negative. In view of the assumed stress partition (Eq. (19)), this is no contradiction.

The equations for hardening rates $\dot{\tau}_y^{(i)}$ deduced from Eqs. (10) and (17)_{2,3} complete the system for the HPT uniform shear in the plane-strain rigid-plastic approximation

$$\begin{aligned}\dot{\tau}_y^{(1)} &= \frac{L_{xy}}{\sin 4\phi} (H_{11} | -\sin 2\phi_2 | + H_{12} | \sin 2\phi_1 |), \\ \dot{\tau}_y^{(2)} &= \frac{L_{xy}}{\sin 4\phi} (H_{21} | -\sin 2\phi_2 | + H_{22} | \sin 2\phi_1 |).\end{aligned}\quad (24)$$

For a given velocity gradient $L_{xy}(t)$ of a HPT test, the slip system orientation angles $\phi_1(t)$, $\phi_2(t)$ and the slip rates $\dot{\gamma}^{(1)}(t)$, $\dot{\gamma}^{(2)}(t)$ follow from Eqs. (17) and (18). The stress response, $S_{xy}(t)$ and $S_{yy}^c(t)$, is governed by Eqs. (21), (22) and (24).

5. Microstructure formation

The simplified model restricted to homogeneous deformation that has been analyzed in the previous sections has revealed three essential features of the HPT deformation:

- (i) To satisfy the imposed HPT loading conditions, the slip systems have to rotate and change their activities during the deformation process.
- (ii) The rotation approaches the single slip orientation of simple shear, which provides a base for the steady-state saturation.
- (iii) The high axial compression is needed mainly to provide the axial stress component that keeps the slip systems active.

To incorporate the fragmentation, the model has to be generalized to inhomogeneous deformation. The first theoretical model of fragmentation within the framework of continuum mechanics was proposed by Biot [12], who treated formation of misoriented structural elements as an instability of homogeneous deformation. The application to crystal plasticity [13] has been developed into a systematic theory in papers [10,6]. The essence of the fragmentation mechanism is shown in Fig. 8, which visualizes the results of the detailed analysis of symmetric double slip deformation in a tension test. In Fig. 8, one out of four misoriented cells is sheared by double slip, two cells are deformed by single slip and the last one remains undeformed. The reason for fragmentation is a minimization of the free and dissipative energy during the deformation process. As in most cases the double slip leads to more hardening than a single slip, the crystal tries to decrease locally the number of active slip systems. For this reason, the microstructure shown schematically in Fig. 8 is energetically favorable compared to a homogeneous deformation carried by double slip. As already noted by Biot [12], the

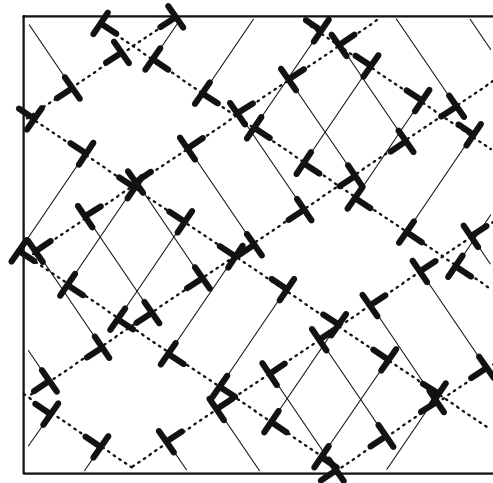


Fig. 8. Visualization of the misoriented microstructure in symmetric double slip [9].

standard continuum mechanics, which contains no length scale, predicts the zero cell size as it leads to the lowest energy. However, the mutually rotated cells fit together by means of excess dislocations (usually called geometrically necessary dislocations, GNDs) forming the cell boundaries. To form the boundaries, an interface energy is needed. When the cell size decreases, the number of cells per unit volume, the interface area and the related interface energy all increase. From this point of view, the cell size is a compromise between these two energetically driven tendencies. An approximate formula for the cell size derived in [6] is recalled in the paragraph Structural size below.

Due to its energy minimization nature, the fragmentation process has a general validity applicable to HPT substructure formation. However, the mechanism of misoriented structural elements (cells) manifested in Fig. 8 has been analyzed in the case of symmetric double slip with fixed symmetry axis and the same average slip activity of both slip systems. Neither of these assumptions is valid for HPT: the symmetry axis of the slip systems rotates and the activity of the slip systems is much different. Both these features seem to be essential for the observed strength increase. To our knowledge, no adequate theoretical model has yet been developed. Despite the fact that a corresponding generalization of the model [9,10,6] is still under development, we believe that some general qualitative conclusions can be drawn. Hence, we try in the next few paragraphs to interpret some of the observed phenomena summarized in Section 1.

5.1. Preferred alignment

As derived in [6] and shown in Fig. 8, two superposed sets of periodically arranged parallel bands, symmetrically oriented with respect to the tensile axis, form a pattern of misoriented dislocation cells. The orientations of the bands deviate from the slip directions; however, they retain double-slip symmetry. Orientation depends in a complex way

on the angle between the slip systems 2ϕ , on the hardening matrices (an analogy of the present hardening coefficients H_{ij}) and on the pre-stress (an analogy of the present stress \mathbf{S}). The symmetry axis of the double slip that coincides with the tensile axis represents a preferred alignment of the cell pattern.

In HPT, the symmetry axis of the double slip rotates with the slip systems toward $\pm(90^\circ - \phi)$, which corresponds to the stable slip orientations. In analogy to Fig. 8, we can expect the cell pattern in the radial direction of HPT to follow this symmetry axis. As, in HPT, the slips in the individual slip systems differ and their distribution varies (see Eq. (17) and Fig. 5), the preferred alignment of the cell pattern need not coincide with the symmetry axis direction. Nevertheless, a tendency of the cell pattern to follow the orientation of the slip systems might be a reason for the observed preferred alignment of the structural elements inclined with respect to the torsion axis [2]. This hypothesis is supported by the results of the cyclic HPT [3], where the direction of the preferred alignment changes with the reverse of the twist. The proposed model exhibits a similar feature: the reverse of the applied shear rotates the slip systems in the opposite direction and the newly formed cell pattern would tend to form a mirror preferred alignment.

5.2. Misorientations

The model presented in [6] predicts that the misorientation increases with strain. In the case of the HPT model, we can expect similar increase in the cell misorientation. However, unlike the observed tendency to randomly distributed large misorientations [2], the modeled misorientations are small periodic deviations from the uniform orientation. From the proposed HPT model, one can deduce that the boundaries between adjacent cells may have a special structure that is different from the standard grain boundaries. At each orientation of the slip systems, there is a tendency to build a particular cell pattern. Due to the rotation of the systems, these patterns may overlap. This might be a reason for formation of the observed dislocation layers of finite thickness separating the cells, the so-called ‘non-equilibrium boundaries’. According to this hypothesis, the boundaries formed in later stages of deformation, where the rate of rotation per applied shear strain diminishes, should be better defined and be akin to the ‘true’ grain boundaries.

5.3. Structural size

The plane-strain model of symmetric double slip of a crystal in tension [6] has provided an order of magnitude estimate of the cell size expressed by the factor R (Eq. (75) in Ref. [6]):

$$R \approx \frac{GD}{\kappa\rho\delta}, \quad (25)$$

where G is the shear modulus, D is the non-local hardening parameter, deduced from dislocation statistics to be of order $D \approx 1$, κ represents the local hardening expressed in the present model by the hardening coefficients H_{ij} , ρ is the total density of dislocations in the cell boundaries and δ is the width of the boundaries. The order of magnitude estimate of R for values characteristic of metal crystals in tension is: $G = 3 \times 10^{10}$ Pa, $\kappa \approx 10^8$ Pa, $\delta \approx 10^{-9}$ m and $10^{15} \text{ m}^{-2} < \rho < 10^{17} \text{ m}^{-2}$. R is in the range $3 \mu\text{m} < R < 300 \mu\text{m}$. If, for an estimate of the structural size in HPT, we employ the same approach, we can expect no change in G and D , as both are of an elastic nature. On the other hand, the observed non-equilibrium boundaries are wider than $\delta \approx 10^{-9}$ m of standard grain boundaries. The rotation of the slip system may have a similar effect to a change in loading trajectories³. Changes in deformation microstructure caused by simple shear in steel pre-deformed in tension were studied in [14]. It was observed that the new dislocation cells correlated to the subsequent loading gradually replace the cell structure caused by the pre-strain. Dislocation structures resulting from tension vanish when the shear strain exceeds the pre-strain amount. In HPT, the rotation of the slip systems may cause a continuous replacement. It might be that non-equilibrium boundaries are less suitable as annihilation centers increasing hardening and the dislocation density. Therefore, there is a reason to suppose that the denominator in (25) for HPT is significantly larger than in conventional tests, hence, the structural size becomes smaller. It must be emphasized, however, that the estimate (25) predicts neither the evolution nor the saturation of the pattern size.

5.4. Saturation

Within the framework of the proposed model, the saturation is related to the states of stable orientation, $\phi_1 = \pm 90^\circ$. These states are approached from all initial orientations of the slip systems. In Fig. 6, it is seen that, for the initial orientation $\phi_1(0) = 0^\circ$, the shear needed to approach the stable state is $F_{xy} \sim 2$. For $-20^\circ < \phi_1(0) < 0^\circ$ the shear becomes larger, whereas for $0^\circ < \phi_1(0)$ the needed shear F_{xy} decreases. These values are an order of magnitude smaller than the reported values of the saturated strain [2]. However, two additional processes might be involved. A certain amount of strain is needed to reach the orientation of the quasi-double slip, similar to the case of PSC [8]. Moreover, a saturated steady state needs to build a microstructure in which generation and annihilation of dislocations are in equilibrium. The matured microstructure of the saturated state should either provide a sufficient density of effective generation–annihilation centers within the cell boundaries or build additional

³ In [15], it was demonstrated that the stress is highest for a ‘circular’ continuous change of loading trajectories.

accidental annihilation centers. This tendency seems to determine the saturated microstructure.

5.5. Fragmentation in axial direction

As has been already mentioned, the assumption of the plane-strain double slip excludes the fragmentation seen in the axial direction. The most distinguished feature related to the axial cell pattern is the gradient of plastic strain in the radial direction. Using the estimate $\gamma = r\theta/h$ and $\nabla\gamma = \theta/h = b\rho_G$, we get $\rho_G = \gamma/(r b)$, where θ is the twist angle, h is the height of the cylindrical specimen, r is the distance from the torsion axis, ∇ is the gradient in the radial direction, $b = 2.5 \times 10^{-10}$ m is the magnitude of the Burger vector and ρ_G is the density of GNDs. For representative values $r = 2$ mm (in [2] specimens were cut at $r = 1.5$ mm and $r = 3$ mm from the torsion axis) and $\gamma = 10$, the estimate gives $\rho_G = 2 \times 10^{13}$ m⁻². In the plane-strain approximation used in the previous section, the GNDs of the cell boundaries seen in the radial direction have an edge character. From this point of view, GNDs in the axial direction could be modeled as screw parts connecting the edge segments to form dislocation loops. Due to the radial gradient nature of the cell arrangement as seen in the axial direction, there is no reason for a preferred alignment, as already observed in [2].

6. Summary

- In the present analysis, the observation reported in Ref. [5] that the HPT shearing imposed by torsion was achieved by an intergranular glide has been accepted as a principle guideline.
- The evolution of the HPT microstructure observed in sections perpendicular to the radial direction has been studied as simple shear carried by double slip. The most clearly distinguished feature relating to the HPT microstructure as observed in the axial direction is the radial gradient of shear strain.
- The basic feature of the modeling of the microstructure in the radial direction is a rotation of the slip systems carrying the imposed shear strain. The orientations of the slip systems asymptotically approach a steady state of single slip.
- The analysis indicates that the high axial compression is needed mainly to provide the axial stress component to keep the slip systems active and to preserve the contact between the specimen and the tool.

The present knowledge about the mechanism of the observed fragmentation into the misoriented structural elements is incomplete; nevertheless, it suggests the interpretation of some HPT observations:

- The formation of the misoriented structural elements can be explained as a result of a trend to reduce the energetically costly multislip. This means that at each slip system orientation there is a tendency to build a corresponding pattern with a locally reduced number of slip systems.
- The rotation of the slip systems causes a continuous reconstruction of the pattern. The necessary destruction of the previous pattern can lead to an increase in the dislocation density and enhanced hardening.
- The asymptotically reached steady state of the lattice rotation may be related to the observed saturation effect.
- A tendency of the pattern to follow the orientation of the rotating slip systems might be a reason for the observed preferred alignment of the structural elements inclined with respect to the torsion axis as observed in the radial direction.
- The size of the structural elements is a result of the competition between two tendencies: during the deformation process, the internal and dissipative energy tends to decrease the structural size, whereas the interface energy of the cell boundaries opposes this trend.

Acknowledgements

We are grateful to Prof. R. Pippan for inspiring discussions, and providing information on HPT and valuable comments on the manuscript. Thanks are also due to Prof. E. Werner for critically reading the text. Finally, we thank the anonymous referee for his/her comments and suggestions. The research was supported by Grants VZ-MŠMT 6840770003 (J.K.) and VZ-MŠMT 6840770021 (M.K.).

References

- [1] Valiev RZ, Islamgaliev RK, Alexandrov IV. *Progr Mater Sci* 2004;45:103.
- [2] Hebesberger T, Stüwe HP, Vorhauer A, Wetscher F, Pippan R. *Acta Mater* 2005;53:393.
- [3] Wetscher F, Pippan R. *Philos Mag* 2006;86:5867.
- [4] Hafok M, Pippan R. *Mater Sci Forum* 2007;550:277.
- [5] Hafok M, Pippan R. *Scr Mater* 2007;56:757.
- [6] Kratochvíl J, Kružík M, Sedláček R. *Phys Rev B* 2007;75:064104.
- [7] Asaro RJ. *J Appl Mech* 1983;50:921.
- [8] Harren SV, Dève HE, Asaro RJ. *Acta Metall* 1988;36:2435.
- [9] Sedláček R. Instability origin of subgrain formation. PhD thesis, Universität Erlangen-Nürnberg, Erlangen, 1999.
- [10] Sedláček R, Kratochvíl J, Blum W. *Phys Stat Sol* 2001;186:1.
- [11] Ecker W. Simulation eines Hochdruck-Torsions-Versuches zum Zwecke der Kalibrierung von Werkstoffdaten von Schienenmaterial. Master's thesis, Montanuniversität Leoben, Leoben, 2004.
- [12] Biot MA. *Mechanics of incremental deformations*. New York: Wiley; 1965.
- [13] Kratochvíl J, Orlová A. *Philos Mag* 1990;A61:281.
- [14] Rauch EF, Schmitt JH. *Mater Sci Eng A* 1989;113:441.
- [15] Tanaka E, Murakami S, Ooka M. *J Mech Phys Solids* 1985; 33:559.